Optical Materials 42 (2015) 319–324

Contents lists available at ScienceDirect

Optical Materials

journal homepage: www.elsevier.com/locate/optmat

Down-shifting spectroscopic properties of Yb^{3+} doped $BaGd_2ZnO_5$ phosphors

Yanmin Yang [a], Linlin Liu [a], Mingming Li [a], Chao Mi [a], Yanzhou Liu [a], Qinglin Guo [a,*], Yi Zhang [b], Xihong Fu [c], Shuzhen Cai [a], Yaohua Mai [a,*]

[a] Hebei Key Lab of Optic-Electronic Information and Materials, College of Physics Science and Technology, Hebei University, Baoding 071002, China
[b] Institute of Photo-Electronic Thin Film Devices and Technology, Tianjin Key Laboratory of Photo-Electronic Thin Film Devices and Technology, Nankai University, Tianjin 300071, China
[c] Lab of Excited State Processes, Changchun Institute of Optics, Fine Mechanics and Physics, Chinese Academy of Sciences, Changchun 130033, China

ARTICLE INFO

Article history:
Received 13 October 2014
Received in revised form 18 December 2014
Accepted 19 January 2015
Available online 7 February 2015

Keywords:
Broad-band absorption
Narrow-band emission
Energy transfer
Solar cells

ABSTRACT

Yb^{3+} doped $BaGd_2ZnO_5$ phosphor was synthesized via sol–gel method. X-ray diffraction, scanning electron microscopy and photoluminescence spectra were employed to characterize the as-obtained products. Upon 274 nm excitation, a single strong narrow-band emission from $^2F_{5/2} \rightarrow {}^2F_{7/2}$ of Yb^{3+} ion around 977 nm was obtained in Yb^{3+} doped $BaGd_2ZnO_5$ phosphor, which was well suited to efficient absorption in a silicon solar cell. After adding Ce^{3+} into Yb^{3+}-doped $BaGd_2ZnO_5$, the excitation spectra of samples monitored at 977 nm indicated that the excitation peaks were in the broad range from 230 nm to 400 nm, which covered ultraviolet and blue light with poor solar cell spectral response. Furthermore, Er^{3+} was introduced into Yb^{3+}-doped $BaGd_2ZnO_5$ phosphor to prove the high energy transfer efficiency from Gd^{3+} ion to Yb^{3+} ion by comparing it with that of Er^{3+} ion to Yb^{3+} ion. With access to broad-band absorption, narrow-band emission as well as high energy transfer efficiency, Ce^{3+}, Yb^{3+}-codoped $BaGd_2ZnO_5$ may have potential applications in modifying the solar spectrum to enhance the efficiency of silicon solar cells.

1. Introduction

The conversion from sunlight to electricity using solar cell devices represents a promising approach to green and renewable energy generation. Spectral mismatch between the photon energy of incident solar radiation and the semiconductor bandgap is an important limiting factor for the solar cell conversion efficiency [1–3]. Trupke [4] proposed an effective method to improve solar cell efficiencies by down-conversion (DC) of high-energy photons, which adapted the solar spectrum to split one higher energy photon to two photons with a smaller energy (usually near-infrared (NIR) photons), and these photons can be absorbed subsequently by the solar cell and generate an electron–hole pair. Richards [5] has predicted that DC in conjunction with a silicon solar cell can achieve a conversion efficiency up to 38.6%. Rare-earth (RE) doped DC luminescent materials are extensively used in the lighting industry, as well as in the fabrication of cathode ray tubes (CRT), plasma display panel (PDP), and white-light emitting diodes (W-LED) technologies [6–14]. The motivation for using rare-earths is that their luminescence covers a wide range, from the near-infrared (NIR), through the visible (VIS) to the ultraviolet (UV). Recently, RE ions doped DC luminescent materials, such as Er^{3+}–Yb^{3+} [15–18], Ho^{3+}–Yb^{3+} [19–20], Tm^{3+}–Yb^{3+} [21–22], Nd^{3+}–Yb^{3+} [23], Dy^{3+}–Yb^{3+} [24], and Tb^{3+}–Yb^{3+} [25–28] are used in solar cells to improve solar energy conversion efficiencies. However, their optical transitions involve 4f orbits, which are well shielded from their local environment by the outer completely-filled $5s^2$ and $5p^6$ orbits, so the emission from the RE ions is line-like. Transitions between different f levels are parity forbidden, and hence the absorption coefficients are low (typically a few cm^{-1}) and the lifetime is long [29]. It is well known that the internal quantum efficiency (IQE) can be up to approximately 200% [17,30] in RE ions doped DC luminescent materials. In practice, the external quantum efficiency (EQE) is much less than 100% due to low absorption coefficients of rare earths. Furthermore, narrow-band absorption leads to only a small part of solar energy that can be converted into electricity. The pathway to decrease the population of high energy levels is not unique, which results in low EQE, too.

There is another approach to improve solar cell efficiencies by down-shifting (shifting one short wavelength photon into a long

* Corresponding authors. Tel./fax: +86 159 3028 4830.
E-mail addresses: yangym@hbu.edu.cn (Q. Guo), mihuyym@163.com, yaohuamai@163.com (Y. Mai).

http://dx.doi.org/10.1016/j.optmat.2015.01.021
0925-3467/

wavelength photon which can be better accepted by the solar cell), which is one of the DC. Furthermore, the DC also includes quantum cutting which refers to transferring one high energy photon into two or more low energy photons. In contrast with DC, a solar cell with a down-shifting material does not have a larger limiting efficiency than a single junction solar cell. The concept can, however, be useful for industrial type solar cells which have a poor blue response, by shifting the spectrum towards wavelengths with a higher IQE. One important reason why down-shifting materials can be used for solar cells is its broad absorption band, which leads to higher EQE. What is exciting is that the absorption transition of Ce^{3+} and Eu^{2+} allows electric dipole transition from 4f ground state to 5d excited state with a very high absorption cross section in an order of 10^{-18} cm^2 in ultraviolet(UV) region. Therefore, the Ce^{3+}/Eu^{2+}–Yb^{3+} couple is an ideal NIR QC system as a solar spectral converter for c-Si solar cell [31–36], as shown in Fig. 1, it depicts the broad band absorption and narrow band emission process, and the mismatching between the solar spectra and the Silicon response.

In this paper, photoluminescence (PL) of $BaGd_2ZnO_5$:Yb^{3+} prepared via sol–gel method was researched through the emission spectra, excitation spectra and energy level diagram. According to the obtained data, we believe that the energy transfer from $BaGd_2ZnO_5$ host to Yb^{3+} occurs. The excitation spectra can be widened by introducing Ce^{3+} ion. $BaGd_2ZnO_5$: Ce^{3+}, Yb^{3+} can be used to improve the efficiencies of silicon solar cells.

2. Experimental

2.1. Sample preparation

To study down-shifting of the phosphors, $BaGd_2ZnO_5$: Ce^{3+}, Yb^{3+} were synthesized via sol–gel method. Firstly, $Gd(NO_3)_3$, $Ce(NO_3)_4$ and $Yb(NO_3)_3$ are obtained with HNO_3, Gd_2O_3 (99.99%), CeO_2 (99.99%) and Yb_2O_3 (99.99%). The redundant HNO_3 was removed by heating and evaporation. Then, $Ba(NO_3)_2$, $Zn(NO_3)_2{\cdot}6H_2O$ and above-mentioned nitrate solutions are dissolved in de-ionized water and stirred until solution settles. Subsequently, the citric acid and ethylene glycol are added into the mixture (the molar ratio of the metal, citric acid and ethylene glycol is 1:1:2) and thoroughly stirred for 1.5 h at 70 °C. The mixture is heated for 16 h at 80 °C in a vacuum oven. The polymeric foam obtained is slowly heated to 400 °C for 2 h in the muffle furnace to decompose the organic material. After being ground adequately with the mortar, the powder is heated at a temperature up to 1200 °C for 2 h. Finally, the powder is taken out and ground again, and $BaGd_2ZnO_5$: 1 mol%Ce^{3+}, x mol%Yb^{3+} (x = 0, 1) were obtained. The sol–gel synthesis process of $BaGd_2ZnO_5$ has been given in our previous paper [37]. $BaGd_2ZnO_5$ doped with x%Yb^{3+} (x = 0.1, 0.5, 1, 3, 10, 30) as well as $BaGd_2ZnO_5$: 1%Er^{3+}, x%Yb^{3+} (x = 0, 1, 5) were prepared with the same method.

2.2. Characterization

X-ray diffraction (XRD) is carried out in the 2θ range of 20°–80° using a Bruker D8 advance X-ray diffractometer (Bruker Optics, Ettlingen, Germany) with Cu Kα radiation. The morphology and the size of the obtained samples were observed with field emission-scanning electron microscopy (FE-SEM, JSM-6700F, JEOL). The emission spectra and excitation spectra were measured by the combined time resolved and steady state fluorescence spectrometers (FLS920, Edinburgh Instruments) equipped with two photomultiplier tubes (PMT) (Hamamatsu R928P and a nitrogen cooled (77 K) R5509-73), as well as continuous wavelength 450 W ozone free xenon (Xe) lamp as excitation source.

3. Results and discussion

3.1. Crystal structure

The SEM image of the $BaGd_2ZnO_5$ is shown in Fig. 2. It can be seen that the nanoparticles have the same rod-like morphology and sizes. The average diameter of the nanoparticles is about 500 nm. Fig. 3 displays the Rietveld refinement plot with the XRD pattern of $BaGd_2ZnO_5$: 1%Er^{3+}, 5%Yb^{3+} Phosphor. This indicates that no impurity phase is presented in the as-prepared

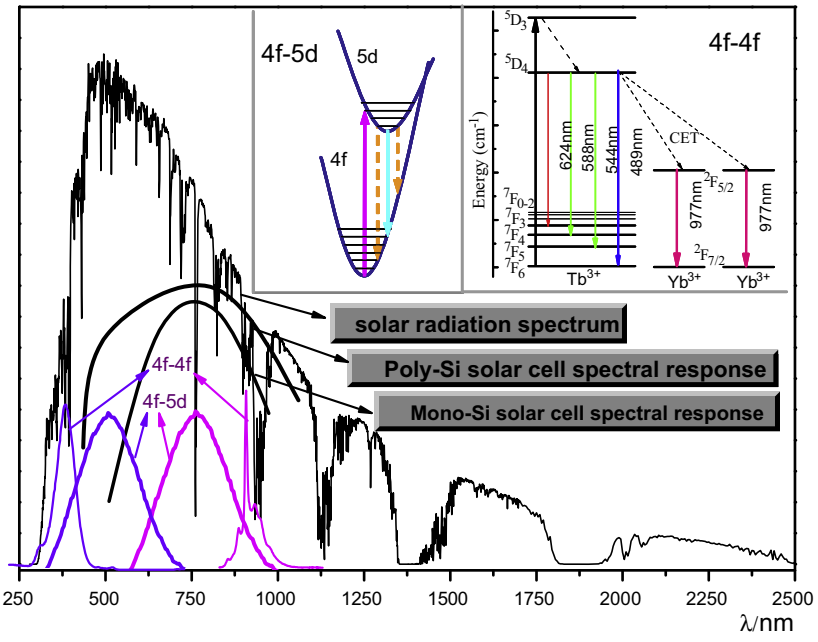

Fig. 1. The solar radiation spectrum, polycrystalline silicon (Poly-Si) and monocrystalline silicon (Mono-Si) solar cell spectral response curves, RE ions sharp line spectra and broadband spectra; Inset gives the corresponding energy level of RE ions. (The data are from our previous work [37]).

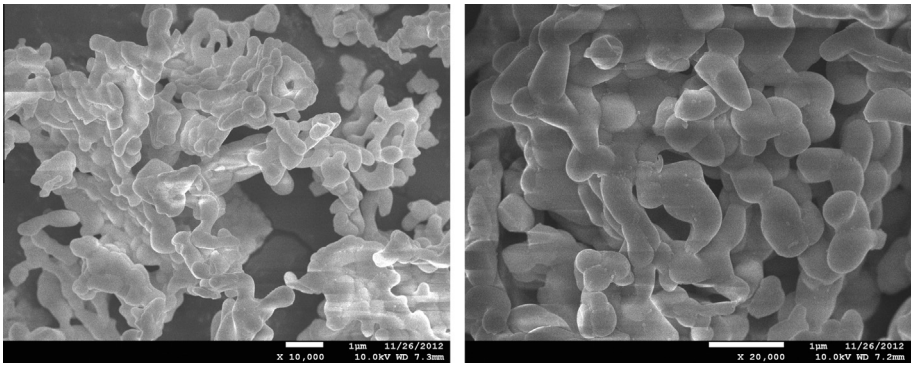

Fig. 2. The SEM micrographs of the $BaGd_2ZnO_5$ sample with different amplification factors.

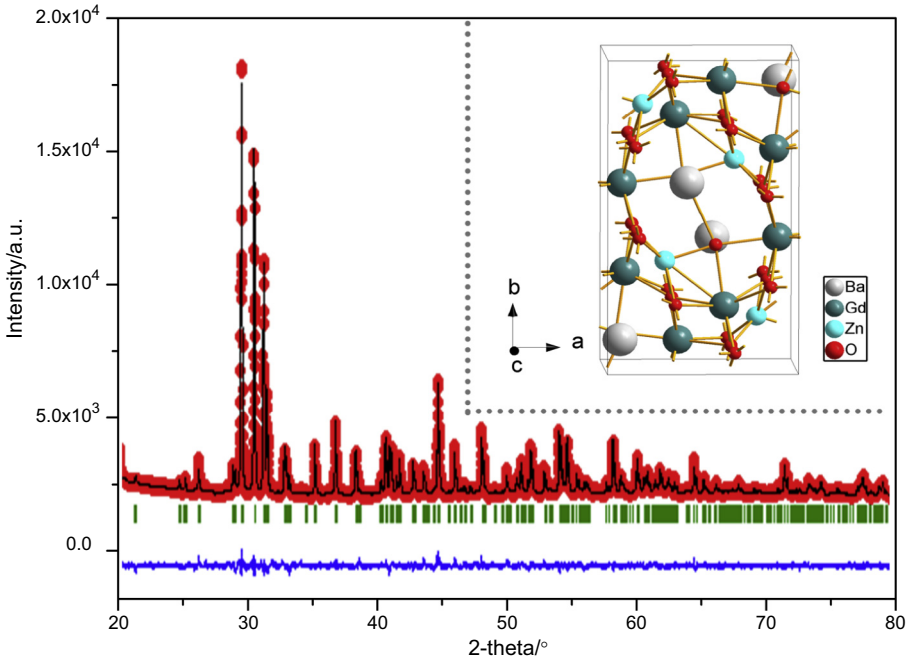

Fig. 3. Final Rietveld refinement plots of $BaGd_2ZnO_5$: 1%Er^{3+}, 5%Yb^{3+}. Small circles (o) correspond to experimental values, and the continuous lines, the calculated pattern; vertical bars (|) indicate the position of Bragg peaks. The bottom trace depicts the difference between the experimental and the calculated intensity values. The inset is crystal structure of $BaGd_2ZnO_5$ seen from the *c* axis.

powders and the host crystal structure is not changed by doping Er^{3+} and Yb^{3+}. The inset in Fig. 3 shows the crystal structure schematic of $BaGd_2ZnO_5$ seen from the c axis, which belongs to the orthorhombic structure. The fractional atomic coordinates for $BaGd_2ZnO_5$: 1%Er^{3+}, 5%Yb^{3+} are reported in Table 1. The crystallographic data, experimental details of X-ray powder diffraction, and Rietveld refinement data for $BaGd_2ZnO_5$: 1%Er^{3+}, 5%Yb^{3+} are reported in Table 2. From this table, the lattice constants of $BaGd_2ZnO_5$: 1%Er^{3+}, 5%Yb^{3+} are: $a = 7.148$ Å, $b = 12.478$ Å, $c = 5.767$ Å and $V = 514.39$ Å^3, which is slightly smaller than that

Table 1
Fractional atomic coordinates for $BaGd_2ZnO_5$: 1%Er^{3+}, 5%Yb^{3+} obtained from the Rietveld refinement using X-ray powder diffraction data at room temperature.

Atom	Site	*x*	*y*	*z*	Occupancy
Ba	4c	0.89927	0.93283	0.25000	0.500
Gd1	4c	0.07806	0.26460	0.25000	0.500
Gd2	4c	0.39800	0.03510	0.25000	0.470
Yb	4c	0.39800	0.03510	0.25000	0.025
Er	4c	0.39800	0.03510	0.25000	0.005
Zn	4c	0.81151	0.67221	0.25000	0.500
O1	8d	−0.12394	0.34926	−1.13184	1.000
O2	8d	0.34587	0.41828	0.48915	1.000
O3	4c	0.16410	0.76362	0.25000	0.500

Table 2
Crystallographic data, experimental details of X-ray powder diffraction and Rietveld refinement data for $BaGd_2ZnO_5$: 1%Er^{3+}, 5%Yb^{3+}.

Formula	$BaGd_{0.94}Er_{0.01}Yb_{0.05}ZnO_5$
Radiation type	Cu Kα
2θ range/°	20–80
Symmetry	Orthorhombic
Space group	Pbnm
a/Å	7.1480
b/Å	12.4780
c/Å	5.7673
Volume/Å^3	514.39
Z	4
R_{Bragg} (%)	7.81
R_p (%)	17.5
R_{wp} (%)	13.1
R_{exp} (%)	9.08
χ^2	3.18

of the blank $BaGd_2ZnO_5$. This is attributed to the replacement of Gd^{3+} ions by Er^{3+} and Yb^{3+} ions, which have smaller ion radii. The final agreement factors are shown in Table 2: $R_{Bragg}(\%) = 7.81$, $R_p(\%) = 17.5$, $R_{wp}(\%) = 13.1$, $R_{exp}(\%) = 9.08$ and $\chi^2 = 3.18$. It indicates that the refinement results are good.

3.2. Fluorescence spectra

Fig. 4 (B) shows the emission spectra of $BaGd_2ZnO_5$: $x\%Yb^{3+}$ ($x = 0.1, 0.5, 1, 3, 10, 30$). With increasing Yb^{3+} ion concentrations, the luminescence intensities of emission spectra increase, and the luminescence intensity is the strongest when Yb^{3+} concentration reaches up to 1%. When increasing the concentration of Yb^{3+} from 1% to 30%, the emission intensities gradually decrease because of concentration quenching, which is shown in Fig. 4(C). Furthermore, the excitation spectra of $BaGd_2ZnO_5$: $x\%Yb^{3+}$ ($x = 0.1, 0.5, 1, 10, 30$) are also measured, as shown in Fig. 4(A), and the variety of the luminescence intensity is the same as the emission spectra. It is worth mentioning that when the samples are excited with 274 nm light, no other emission is found expect for 977 nm emission, which can be attributed to $^2F_{5/2} \rightarrow {}^2F_{7/2}$ transition of Yb^{3+} ion. The excitation spectra monitored at 977 nm have two peaks located in 261 nm and 274 nm, respectively. The peak of 274 nm can be ascribed to the transition of $^8S_{7/2} \rightarrow {}^6I_J$ of Gd^{3+} ion. If one photon from $^8S_{7/2}$ level of Gd^{3+} ion translates energy directly to $^2F_{5/2}$ level of Yb^{3+} ion, three photons can be generated and the IQE can be up to approximately 300%. However, the luminescence lifetime of Gd^{3+} cannot be measured, so we cannot prove the three-photon process. The peak of 261 nm can be ascribed to the charge-transfer state absorption of Yb^{3+}, which involves the transfer of an electron from the surrounding $2p^6$ orbital of O^{2-} to the $4f^{13}$ orbital of Yb^{3+} [35,38]. The energy transfer from the $BaGd_2ZnO_5$ host to Yb^{3+} is proved by the excitation and emission spectra.

Yb^{3+} doped $BaGd_2ZnO_5$ can transform UV-light into near-infrared light, which can be used to improve the efficiencies of silicon solar cells. The energy transfer (ET) efficiency is an important parameter. To illustrate the ET efficiency, Er^{3+} ion is introduced into Yb^{3+} doped $BaGd_2ZnO_5$ because $^4I_{11/2}$ level of Er^{3+} ion is resonance energy level with $^2F_{5/2}$ level of Yb^{3+} ion, as shown in Fig. 5. The down-conversion ET from Er^{3+} to Yb^{3+} has been reported in many literatures [15–18], and the ET efficiency is very high.

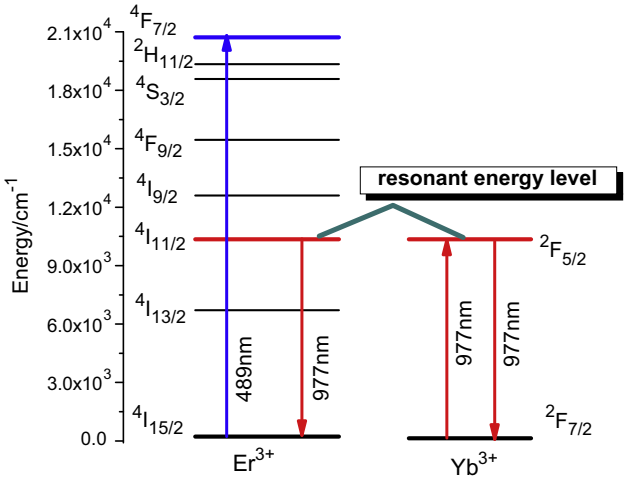

Fig. 5. The resonant energy level of Er^{3+} ($^4I_{11/2}$) and Yb^{3+} ($^2F_{5/2}$).

Fig. 6 shows the emission spectra of $BaGd_2ZnO_5$: $1\%Er^{3+}$, $x\%Yb^{3+}$($x = 0,1$). Compared with the singly Er-doped sample, the Er^{3+}–Yb^{3+} codoped sample has a broader 977 nm emission peak, which is in accordance with the typical emission peak of Yb^{3+}. We can obtain the ET efficiency from Gd^{3+} ion to Yb^{3+} ion by comparing it with that from Er^{3+} ion to Yb^{3+} ion. Fig. 7 shows the excitation spectra of $BaGd_2ZnO_5$: $1\%Er^{3+}$ ($\lambda_{em} = 865$ nm, Er^{3+}:$^4S_{3/2} \rightarrow {}^4I_{13/2}$) and $BaGd_2ZnO_5$: $1\%Er^{3+}$, 1% Yb^{3+} ($\lambda_{em} = 977$ nm, Yb^{3+} $^2F_{5/2} \rightarrow {}^2F_{7/2}$). As is shown in Fig. 7, the peaks around 378 nm ($^4G_{11/2}$), 521 nm ($^2H_{11/2}$) and 652 nm ($^4F_{9/2}$) are the characteristic excitation peaks of Er^{3+} through the excitation spectra of $BaGd_2ZnO_5$: $1\%Er^{3+}$. From the excitation spectra of $BaGd_2ZnO_5$: $1\%Er^{3+}$, 1% Yb^{3+}, we can find that the luminescence intensity excited by 274 nm is much stronger than those of 378 nm, 521 nm and 652 nm, so it proves that the ET from $BaGd_2ZnO_5$ to Yb^{3+} is effective.

From Fig. 4, the energy transfer form Gd^{3+} to Yb^{3+} has been proved, and it may be a three-photon process. So, the energy transfer mechanism from $BaGd_2ZnO_5$ to Yb^{3+} can be described as Fig. 8. Gd^{3+} ion absorbs a 274 nm photon by the transition from $^8S_{7/2}$ to

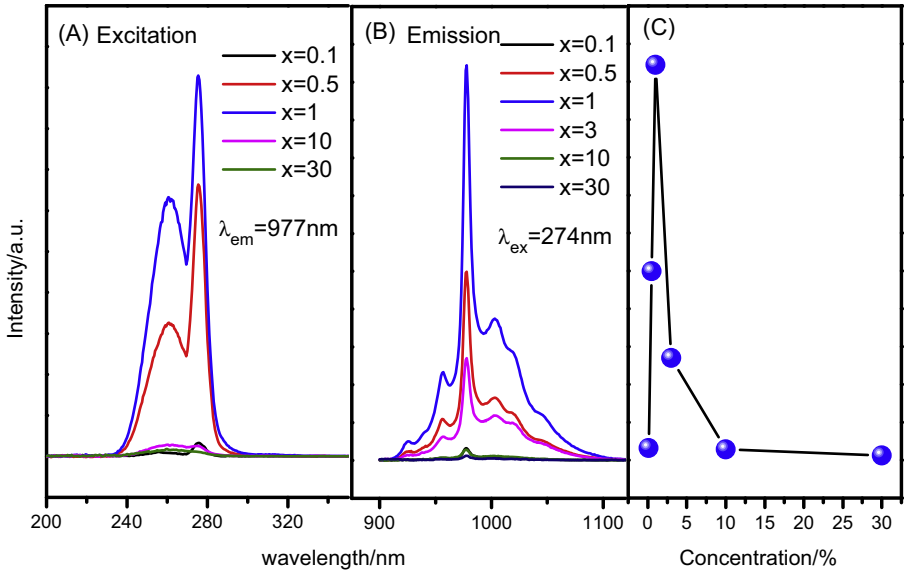

Fig. 4. (A) Excitation spectra of $BaGd_2ZnO_5$ doped with $x\%Yb^{3+}$ ($x = 0.1, 0.5, 1, 10, 30$), (B) emission spectra of $BaGd_2ZnO_5$ doped with $x\%Yb^{3+}$ ($x = 0.1, 0.5, 1, 3, 10, 30$) and (C) the relationship between the luminescence intensity and the Yb^{3+} concentration.

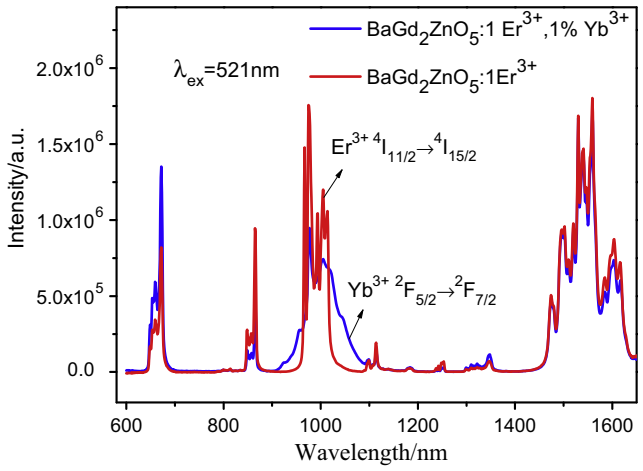

Fig. 6. The emission spectra of $BaGd_2ZnO_5$: 1%Er^{3+}, *x*%Yb^{3+}(*x* = 0, 1).

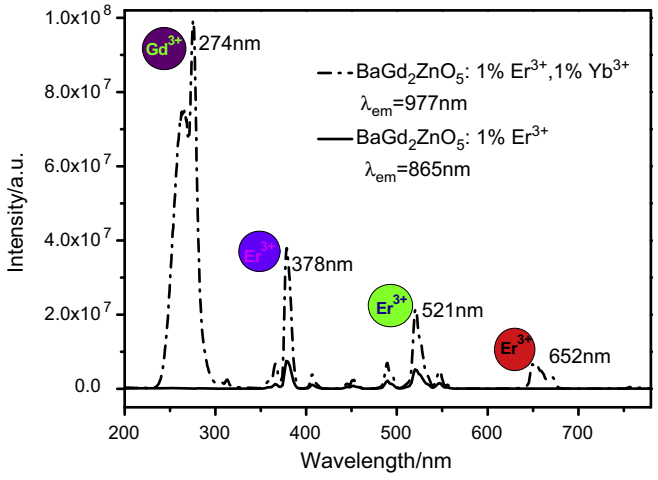

Fig. 7. The excitation spectra of $BaGd_2ZnO_5$: 1%Er^{3+}, 1%Yb^{3+} (λ_{em} = 977 nm) and $BaGd_2ZnO_5$: 1%Er^{3+} (λ_{em} = 865 nm).

^6I_J, and then transfers it to three Yb^{3+} ions and emits three 977 nm photons by $^2F_{5/2} \rightarrow {}^2F_{7/2}$. This ET process from Gd^{3+} to Yb^{3+} has not been reported in previous papers.

The method investigated here for reducing these energy losses is via down-shifting. Yb^{3+}-doped $BaGd_2ZnO_5$ is light-conversion material for solar cell. However, only 200–300 nm light is

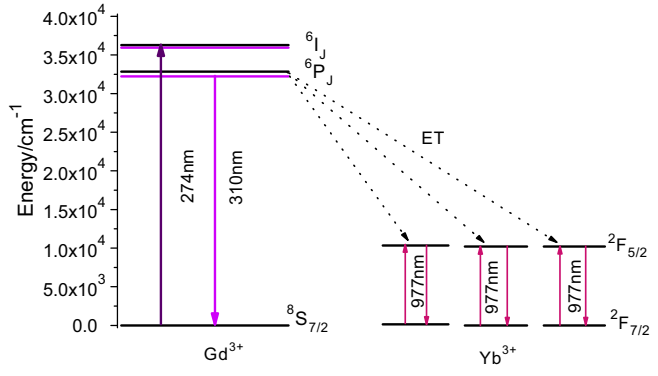

Fig. 8. Energy level diagram of Gd^{3+} and Yb^{3+} scheming the mechanism of energy transfer from $BaGd_2ZnO_5$ to Yb^{3+}.

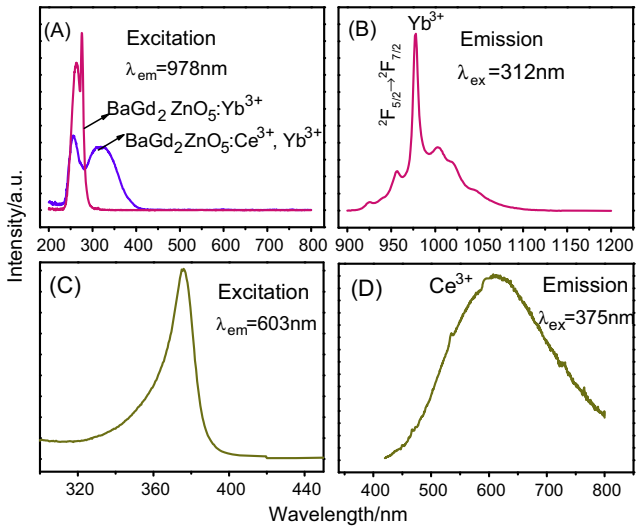

Fig. 9. (A) Excitation spectra of $BaGd_2ZnO_5$:Ce^{3+}, Yb^{3+} and $BaGd_2ZnO_5$: Yb^{3+} (λ_{em} = 978 nm), (B) emission spectrum of $BaGd_2ZnO_5$: Yb^{3+} (λ_{ex} = 274 nm), (C) excitation spectrum of $BaGd_2ZnO_5$: Ce^{3+} (λ_{em} = 603 nm) and (D) emission spectrum of $BaGd_2ZnO_5$: Ce^{3+} (λ_{ex} = 375 nm).

transformed, which is too narrow for Poly-Si as well as Mono-Si solar cell whose spectral response is low at the wavelength range from 200 nm to 500 nm. It is particularly true for Ce^{3+}, whose luminescence is linked to the chemical environment via the crystal field directly [39]. In this paper, Ce^{3+} ion is introduced into Yb^{3+}-doped $BaGd_2ZnO_5$ to investigate the impact of Ce^{3+} on the excitation and emission spectra. Fig. 9(A) shows the excitation spectra of $BaGd_2ZnO_5$: Yb^{3+} and $BaGd_2ZnO_5$: Ce^{3+}, Yb^{3+} monitored at 978 nm (Yb^{3+} $^2F_{5/2} \rightarrow {}^2F_{7/2}$). As can be seen from Fig. 9(A), the excitation spectrum of $BaGd_2ZnO_5$: Ce^{3+}, Yb^{3+} is clearly different from that of $BaGd_2ZnO_5$: Yb^{3+}. First, the characteristic excitation peak of Gd^{3+} at 274 nm is vanished with the introduction of Ce^{3+} ion. Second, a new broad-band absorption, whose peak located at 312 nm covering from 230 nm to 400 nm, appears in the excitation spectrum of $BaGd_2ZnO_5$: Ce^{3+}, Yb^{3+}. Fig. 9 (B) shows the emission spectrum of $BaGd_2ZnO_5$: Ce^{3+}, Yb^{3+} (λ_{ex} = 312 nm), and only a emission peak at 978 nm is obtained, which can be attributed to $^2F_{5/2} \rightarrow {}^2F_{7/2}$ transition of Yb^{3+} ion, no other emission peaks are found. To further analyze the effects of Ce^{3+} ion on the excitation and emission spectra, Ce^{3+} doped $BaGd_2ZnO_5$ was synthesized for purposes of comparison. Fig. 9(C) and (D) show the excitation and emission spectra of Ce^{3+} doped $BaGd_2ZnO_5$, respectively. The characteristic excitation peak of Ce^{3+} is around 375 nm monitored at 603 nm, which does not overlap with that of $BaGd_2ZnO_5$:Ce^{3+}, Yb^{3+} monitored at 978 nm. Furthermore, when excited by 312 nm the characteristic emission peak of Ce^{3+} ion around 603 nm is not observed in the emission spectrum of $BaGd_2ZnO_5$: Ce^{3+}, Yb^{3+}. It indicates that there is no ET from $BaGd_2ZnO_5$ host to Ce^{3+} and the excitation spectrum from 230 nm to 400 nm in $BaGd_2ZnO_5$: Ce^{3+}, Yb^{3+} is not from Ce^{3+} ions.

4. Conclusion

In this work, the samples were prepared via the sol–gel method. The structures of the samples have been proved by the XRD. The emission spectra and excitation spectra were measured and investigated to prove the occurrence of ET from $BaGd_2ZnO_5$ samples to Yb^{3+}, which subsequently led to the 977 nm near-infrared emission. The excitation spectra of $BaGd_2ZnO_5$ doped with Er^{3+} and Yb^{3+} were measured, and it is proved that the ET from $BaGd_2ZnO_5$ to Yb^{3+} is effective. A surprising luminescence of $BaGd_2ZnO_5$ doped

with Ce^{3+} and Yb^{3+} is also investigated. With the addition of Ce^{3+}, a red shift of excitation spectrum occurs, and a broadband excitation spectrum from 230 nm to 400 nm with the peaks at 261 nm and 312 nm is obtained. Because of this amazing phenomenon, this material can be better applied into improving the efficiency of the solar cells.

Acknowledgements

This work was supported by National Science Foundation of China (No. 50902042), China Postdoctoral Science Foundation (No. 20100480840) and Natural Science Foundation of Hebei Province (No. E2010000283). We thank Dr. H. Yang and Dr R. F. Duan of Institute of Semiconductors, Chinese Academy of Science Application R&D Department R&D Center for Semiconductor Lighting; Dr Z. L. Fu of State Key Laboratory of Superhard Materials, College of Physics, Jilin University for their great help in collecting powder X-ray diffraction data, PL measurements.

References

[1] B.M. vander Ende, L. Aarts, A. Meijerink, Lanthanide ions as spectral converters for solar cells, Phys. Chem. Chem. Phys. 11 (2009) 11081–11095.
[2] C. Strümpel, M. McCann, G. Beaucarne, V. Arkhipov, A. Slaoui, V.S. Vrcek, C. del Cañizo, I. Tobias, Modifying the solar spectrum to enhance silicon solar cell efficiency-An overview of available materials, Sol. Energy Mater. Sol. Cells 91 (2007) 238–249.
[3] W.A. Tisdale, K.J. Williams, B.A. Timp, D.J. Norris, E.S. Aydil, X.Y. Zhu, Hot-electron transfer from semiconductor nanocrystals, Science 328 (2010) 1543–1547.
[4] T. Trupke, M.A. Green, P. Würfel, Improving solar cell efficiencies by down-conversion of high-energy photons, J. Appl. Phys. 92 (2002) 1668–1674.
[5] B.S. Richards, Luminescence layers for enhanced silicon solar cell performance. Down-conversion, Sol. Energy Mater. Sol. Cells 90 (2006) 1189–1207.
[6] X.Y. Huang, X.H. Ji, Q.Y. Zhang, Broadband downconversion of ultraviolet light to near-infrared emission in Bi^{3+}–Yb^{3+}-codoped Y_2O_3 phosphors, J. Am. Ceram. Soc. 94 (2011) 833–837.
[7] K.M. Deng, L. Li, X.T. Wei, Y.H. Chen, C.X. Guo, M. Yin, Near infrared quantum cutting in Yb^{3+}-doped $NaY(WO_4)_2$ phosphor with a high quenching concentration, J. Nanosci. Nanotechnol. 11 (2011) 9489–9493.
[8] E. van der Kolk, P. Dorenbos, K. Krämer, D. Biner, H.U. Güdel, High-resolution luminescence spectroscopy study of down-conversion routes in $NaGdF_4$:Nd^{3+} and $NaGdF_4$:Tm^{3+} using synchrotron radiation, Phys. Rev. B 77 (2008) 125110.
[9] Q.Y. Zhang, X.Y. Huang, Recent progress in quantum cutting phosphors, Prog. Mater Sci. 55 (2010) 353–427.
[10] Y.H. Wang, L.H. Xie, H.J. Zhang, Cooperative near-infrared quantum cutting in Tb^{3+}, Yb^{3+} codoped polyborates $La_{0.99-x}Yb_xBaB_9O_{16}$:$Tb_{0.01}$, J. Appl. Phys. 105 (2009) 023528.
[11] T.J. Lee, L.Y. Luo, B.M. Cheng, W.G. Diau, T.M. Chen, Investigation of Pr^{3+} as a sensitizer in quantum-cutting fluoride phosphors, Appl. Phys. Lett. 92 (2008) 081106.
[12] R.T. Wegh, H. Donker, K.D. Oskam, A. Meijerink, Visible quantum cutting in Eu^{3+}-doped gadolinium fluorides via downconversion, J. Lumin. 82 (1999) 93–104.
[13] J. Zhong, H. Liang, Q. Su, J. Zhou, Y. Huang, Z. Gao, Y. Tao, J. Wang, Luminescence properties of $NaGd(PO_3)_4$: Eu^{3+} and energy transfer from Gd^{3+} to Eu^{3+}, Appl. Phys. B 98 (2010) 139–147.
[14] Z.L. Wang, J.H. Hao, L.W. Helen, J.H. Chan Hao, Down- and up-conversion photoluminescence, cathodoluminescence and paramagnetic properties of $NaGdF_4$:Yb^{3+}, Er^{3+} submicron disks assembled from primary nanocrystals, J. Mater. Chem. 20 (2010) 3178–3185.
[15] V.K. Tikhomirov, V.D. Rodríguez, J. Mé ndez-Ramos, J. del-Castillo, D. Kirilenko, G. Van Tendeloo, V.V. Moshchalkov, Optimizing Er/Yb ratio and content in Er–Yb co-doped glass-ceramics for enhancement of the up- and down-conversion luminescence, Sol. Energy Mater. Sol. Cells 100 (2012) 209–215.
[16] S. Xiao, X. Yang, J.W. Ding, Red and near infrared down-conversion in Er^{3+}/Yb^{3+} co-doped YF_3 performed by quantum cutting, Appl. Phys. B 99 (2010) 769–773.
[17] B. Fan, C. Chlique, O.M. Conanec, X.H. Zhang, X.P. Fan, Near-infrared quantum cutting material Er^{3+}/Yb^{3+} Doped La_2O_2S with an external quantum yield higher than 100%, J. Phys. Chem. C 116 (2012) 11652–11657.
[18] J.J. Eilers, D. Biner, J.T. van Wijngaarden, K. Krämer, H.U. Güdel, A. Meijerink, Efficient visible to infrared quantum cutting through downconversion with the Er^{3+}–Yb^{3+} couple in $Cs_3Y_2Br_9$, Appl. Phys. Lett. 96 (2010) 151106.
[19] H. Lin, D. Chen, Y.L. Yu, A.P. Yang, Y.S. Wang, Near-infrared quantum cutting in Ho^{3+}/Yb^{3+} Codoped nanostructured glass ceramic, Opt. Lett. 36 (2011) 876–878.
[20] L.N. Guo, Y.H. Fang, J. Zhang, Y.Z. Wang, P.Y. Dong, Nano. Near-infrared quantum cutting in Ho^{3+}, Yb^{3+}-codoped $BaGdF_5$ nanoparticles via first- and second-order energy transfers, Res. Lett. 7 (2012) 636.
[21] Q. Zhang, B. Zhu, Y.X. Zhuang, G.R. Chen, X.F. Liu, G. Zhang, J.R. Qiu, D.P. Chen, Quantum cutting in Tm^{3+}/Yb^{3+}-codoped lanthanum aluminum germanate glasses, J. Am. Ceram. Soc. 93 (2009) 654–657.
[22] W. Zheng, H.M. Zhu, R.F. Li, D.T. Tu, Y.S. Liu, W.Q. Luo, X.Y. Chen, Visible-to-infrared quantum cutting by phonon-assisted energy transfer in YPO_4:Tm^{3+}, Yb^{3+} phosphors, Phys. Chem. Chem. Phys. 14 (2012) 6974–6980.
[23] Z.G. Xia, Y. Luo, M. Guan, L.B. Liao, Near-infrared luminescence and energy transfer studies of LaOBr:Nd^{3+}/Yb^{3+}, Opt. Soc. Am. 20 (2012) A722–A728.
[24] Y. Dwivedi, S.B. Rai, Spectroscopic study of Dy^{3+} and Dy^{3+}/Yb^{3+} ions co-doped in barium fluoroborate glass, Opt. Mater. 31 (2009) 1472–1477.
[25] Q.Q. Duan, F. Qin, D. Wang, W. Xu, J.M. Cheng, Quantum cutting mechanism in Tb^{3+}–Yb^{3+} co-doped oxyfluoride glass, J. Appl. Phys. 110 (2011) 113503.
[26] I.R. Martín, A.C. Yanes, J. Méndez-Ramos, M.E. Torres, V.D. Rodríguez, Cooperative energy transfer in Yb^{3+}–Tb^{3+} codoped silica sol–gel glasses, J. Appl. Phys. 89 (2001) 2520–2524.
[27] S. Ye, B. Zhu, J.X. Chen, J. Luo, J.R. Qiu, Infrared quantum cutting in Tb^{3+}, Yb^{3+} codoped transparent glass ceramics containing CaF_2 nanocrystals, Appl. Phys. Lett. 92 (2008) 141112.
[28] J.J. Zhou, Y. Teng, S. Ye, Y.X. Zhuang, J.R. Qiu, Enhanced downconversion luminescence by co-doping Ce^{3+} in Tb^{3+}–Yb^{3+} doped borate glasses, Chem. Phys. Lett. 486 (2011) 116–118.
[29] H. Lin, X.H. Yan, X.F. Wang, Synthesis and blue to near-infrared quantum cutting of Pr^{3+}/Yb^{3+} co-doped Li_2TeO_4 phosphors, Mater. Sci. Eng., B 176 (2011) 1537–1540.
[30] N. Kodama, S. Oishi, Visible quantum cutting through downconversion in $KLiGdF_5$:Eu^{3+} crystals, J. Appl. Phys. 98 (2005) 103515–103515-5.
[31] J. Sun, Y. Sun, J. Zeng, H. Du, Near-infrared quantum cutting in Eu^{2+}, Yb^{3+} co-doped $Sr_3Gd(PO_4)_3$ phosphor, Opt. Mater. 35 (2013) 1276–1278.
[32] J.D. Chen, H. Zhang, F. Li, H. Guo, High efficient near-infrared quantum cutting in Ce^{3+}, Yb^{3+} co-doped $LuBO_3$ phosphors, Mater. Chem. Phys. 128 (2011) 191–194.
[33] Q. Yan, J. Ren, Y. Tong, G. Chen, Near-infrared quantum cutting of Eu^{2+}/Yb^{3+} codoped chalcohalide glasses, J. Am. Ceram. Soc. 96 (2013) 1349–1351.
[34] Z. Liu, J. Li, L. Yang, Q. Chen, Y. Chu, N. Dai, Efficient near-infrared quantum cutting in Ce^{3+}–Yb^{3+} codoped glass for solar photovoltaic, Sol. Energy Mater. Sol. Cells 122 (2014) 46–50.
[35] Y. Teng, J. Zhou, S. Ye, J. Qiu, Broadband near-infrared quantum cutting in Eu^{2+} and Yb^{3+} ions Co-doped $CaAl_2O_4$ phosphor, J. Electrochem. Soc. 157 (2010) A1073–A1075.
[36] W.L. Zhou, J. Yang, J. Wang, Y. Li, X.J. Kuang, J.K. Tang, H.B. Liang, Study on the effects of 5d energy locations of Ce^{3+} ions on NIR quantum cutting process in Y_2SiO_5: Ce^{3+}, Yb^{3+}, Opt. Express 20 (2012) A510–A518.
[37] Y.M. Yang, L.L. Liu, S.Z. Cai, F.Y. Jiao, C. Mi, X.Y. Su, J. Zhang, F. Yu, X.D. Li, Z.Q. Li, Up-conversion luminescence and near-infrared quantum cutting in Dy^{3+}, Yb^{3+} co-doped $BaGd_2ZnO_5$ nanocrystal, J. Lumin. 146 (2014) 284–287.
[38] M. Engholm, L. Norin, D. Åberg, Strong UV absorption and visible luminescence in ytterbium-doped aluminosilicate glass under UV excitation, Opt. Lett. 32 (2007) 3352–3354.
[39] H.L. Zhu, E.Z. Zhu, H. Yang, L.N. Wang, D.L. Jin, K.H. Yao, High-brightness $LaPO_4$:Ce^{3+}, Tb^{3+} nanophosphors: reductive hydrothermal synthesis and photoluminescent properties, J. Am. Ceram. Soc. 91 (2008) 1682–1685.